Journal of Power Sources 203 (2012) 159–164

Contents lists available at SciVerse ScienceDirect

Journal of Power Sources

journal homepage: www.elsevier.com/locate/jpowsour

Manganese oxide with a card-house-like structure reassembled from nanosheets for rechargeable Li-air battery

Shintaro Ida*, Arjun Kumar Thapa, Yuiko Hidaka, Yohei Okamoto, Maki Matsuka, Hidehisa Hagiwara, Tatsumi Ishihara**

Department of Applied Chemistry, Faculty of Engineering, Kyushu University, 744 Motooka, Nishi-ku, Fukuoka 819-0395, Japan

ARTICLE INFO

Article history:
Received 25 August 2011
Received in revised form 3 November 2011
Accepted 15 November 2011
Available online 23 November 2011

Keywords:
Nanosheets
Manganese oxide
Catalyst
Li-air battery

ABSTRACT

Li-air batteries have attracted attention as a next generation secondary battery because of their potentials such as a high theoretical specific energy density. One of the main issues for the Li-air batteries is the development of a cathode oxygen electrode with high capacity and charge–discharge cycle stability. Here we report a manganese oxide with a card-house-like structure for the cathode oxygen electrode. The manganese oxide was synthesized by reassembling two-dimensional manganese oxide nanosheets. The cathode electrode containing the manganese oxide exhibited high catalytic activity for Li^+/Li_2O_x ($x = 1$, 2) redox reactions, and its discharge capacity was 1300–1500 mAh g^{-1} catalyst, which was higher than that of Li-air batteries using electrolytic MnO_2 as catalysts.

1. Introduction

Rechargeable Li-air batteries have attracted considerable attention as high capacity electrical storage devices for the use in electric and hybrid vehicles [1–3]. Among the various known metal-air battery systems, Li-air battery is the most attractive one as it has the highest energy density per unit weight. Its discharge reaction occurs between Li and oxygen to yield Li_2O or Li_2O_2, and a theoretical specific energy density of 5200 Wh kg^{-1}. In practice, the storage of oxygen is not required, since air can be used directly in the battery. Therefore, the theoretical specific energy density (excluding oxygen) is 11,140 Wh kg^{-1}, which is much higher than that of other advanced batteries [4]. In general, a Li-air battery consists of a lithium anode, an air cathode that supplies oxygen, and an electrolyte. Abraham and Jiang reported a Li-air battery using a nonaqueous electrolyte [1]. However, due to the low oxygen solubility in the nonaqueous electrolyte, the reported power density of the Li-air battery was much lower than the theoretical value [5,6]. During the discharge reactions, oxygen is reduced by lithium ions to form lithium peroxide or oxide at the air cathode, while lithium ions dissolve into the electrolyte from the lithium metal anode, as shown in the following reactions.

Cathode (discharge reaction):

$$2Li^+ + 2e^- + O_2 \rightarrow Li_2O_2 \quad (1)$$

$$4Li^+ + 4e^- + O_2 \rightarrow 2Li_2O \quad (2)$$

Anode (discharge reaction):

$$Li \rightarrow Li^+ + e^- \quad (3)$$

Rechargeable Li-air batteries require reversible cathode electrode reactions between the Li_2O_x ($x = 1$, 2) deposition reaction (discharge reaction, reaction of Eqs. (1) and (2)) and the Li_2O_x decomposition reaction (charge reaction) at the cathode (these reactions are complex reactions, and have not been fully understood). However, discharge and charge reactions are still relatively slow for practical applications. Therefore, one of the main issues for the improvement of Li-air batteries is the development of effective catalysts for the both reactions. Recently, MnO_2 [7,8], MnO_2/Pd [9,10], and Pt–Au nanoparticle [11] have been reported as the effective catalysts for this purpose. Another issue is the control of pore size in the cathode electrodes. Lithium oxides and peroxides generated during the discharge reactions precipitate in the pores of the air cathode electrodes, and interfere with further intake of oxygen, which can abruptly terminate the discharge reactions. Thus, the catalytic materials with relatively large pore sizes and surface area are essential to obtain high capacity and charge–discharge cycle stability.

In this study, we report manganese oxide with a card-house-like structure for the cathode oxygen electrode, which was prepared by reassembling manganese oxide nanosheets. This uniquely

* Corresponding author. Fax: +81 928022870.
** Corresponding author. Fax: +81 928022871.
E-mail addresses: s-ida@cstf.kyushu-u.ac.jp (S. Ida), ishihara@cstf.kyushu-u.ac.jp (T. Ishihara).

0378-7753/$ – see front matter © 2011 Elsevier B.V. All rights reserved.
doi:10.1016/j.jpowsour.2011.11.042

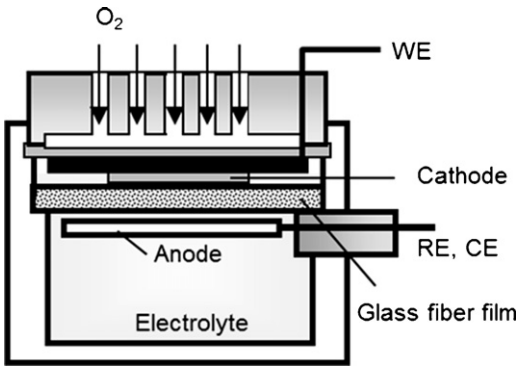

Fig. 1. Structural model of cell.

structured manganese oxide exhibited high catalytic activities for the Li^+/Li_2O_x redox reactions, and the consumption and release of oxygen were confirmed during the Li^+/Li_2O_x redox reactions.

2. Experimental

Manganese oxide nanosheets were prepared by exfoliating layered $K_{0.45}MnO_2$ according to a procedure given in the literature [12]. $K_{0.45}MnO_2$ was prepared by reacting stoichiometric amounts of intimately mixed K_2CO_3 (Wako Pure Chemical Co., Japan; 99.9%) and Mn_2O_3 (Wako Pure Chemical Co., Japan; 99.9%) at 750 °C for 30 h in O_2 gas. Proton exchange reaction of K^+ in the layered manganese oxide was carried out by stirring 1.0 g of $K_{0.45}MnO_2$ powder in 100 mL of 1 M aqueous HCl solution for 7 days at room temperature. Finally, the protonated form (0.4 g) was mixed with 100 mL of 0.05 M tetrabutylammonium hydroxide aqueous solution to exfoliate the host layers, and the resulting suspension was stirred at room temperature for 10 days. The suspension was then centrifuged for 30 min to remove the unexfoliated layered manganese oxide, and the supernatant was used as the nanosheet suspension. Manganese oxide with a card-house-like structure was prepared by drying the suspension of the manganese oxide nanosheets. 50 mL of the nanosheet suspension was placed into an agate mortar, and then heated under an incandescent lamp until reduced by quarter in volume (surface temperature: 80–85 °C). The nanosheets gradually reassembled into mesoporous manganese oxides during the heat treatment, as the concentration of the electrolyte (tetrabutylammonium hydroxide) increased with evaporating the solvent. 35 mL of ethanol was then added to the suspension, and left until the manganese oxide precipitated to the bottom of the mortar. Subsequently, approximately 35 mL of the solvent was absorbed. This process was repeated 5 times to remove the tetrabutylammonium hydroxide. Finally, the solvent was evaporated under an incandescent lamp, and the manganese oxide powder obtained was dried in a vacuum drier at 150 °C.

Two types of manganese oxides with non-card-house like structure were prepared from the manganese oxide nanosheets for comparison. One was prepared by naturally drying of sediment obtained by centrifugation (12,000 rpm, 60 h) of 50 mL of manganese oxide nanosheet suspension. The other one was prepared as follows. The sediment prepared obtained by centrifugation (12,000 rpm, 60 h) of 50 mL of manganese oxide nanosheet suspension was dispersed into water by ultrasonic agitation, and the suspension was freeze-dried. Finally, these manganese oxide powders obtained were dried in a vacuum drier at 150 °C.

The cathode for the Li-air battery was prepared by casting a mixture of the manganese oxide powder, PTFE-coated acetylene black (PTFE: acetylene black = 1:3, Hirota) as the conducting binder, and Ketjenblack (EC600JD) as a conducting material with a total weight ratio of 42:56:2. The resulting mixture was pressed onto a stainless steel mesh, and dried at 160 °C for 12 h in vacuum. Fig. 1 shows the structural model of the cell. A piece of lithium foil (thickness: 0.1 mm) was used as the anode, and was separated by a porous polypropylene film (Mitsubishi Chemical, Celgard 3401). The cell was gas-tight except for the stainless steel mesh windows to expose the porous cathode to the O_2 atmosphere. A mixed solution of 1 M lithium bis-(trifluoromethanesulfonyl) imide, ethylene carbonate (EC), and diethyl carbonate (DEC) (Ube Chemical Co., Ltd., Japan) with a volume ratio (EC:DEC) of 3:7 was used as the electrolyte. It has been widely accepted that carbonate electrolyte, especially propylene carbonate, is decomposed easily. However, we have confirmed that the EC/DEC electrolyte is unlikely to decomposed under less than 4.0 V [9,10]. Therefore, in this present study, the charge–discharge curves were measured in the voltage range of 4.0–2.0 V (current density of 0.05 mA cm^{-2}) to avoid the decomposition of the electrolyte.

X-ray diffraction (XRD) analysis was undertaken with Cu Kα radiation (λ = 1.541 Å, Rigaku Rint 2500). TEM observation was performed using a JEOL 2100 electron microscope operating at an accelerating voltage of 200 kV. Scanning electron micrographs (SEM) were obtained using a Hitachi SU-8000 and Keyence VE-7800 electron microscopes. Specific surface area was determined from nitrogen adsorption–desorption isotherm using Nippon Bell, BELSORP 18PLUS-FS, Japan. Atomic force microscopy (AFM) image was obtained using a SII Nano navi 2.

3. Results and discussion

The cathode electrode of Li-air batteries requires catalytic activities for redox reaction of the Li_2O_x (x = 1, 2) and mesoporous structure with relatively large pore size for the Li_2O_x depositions and continuous diffusion of oxygen. A card-house structure is one of the ideal catalyst structures for the Li^+/Li_2O_x redox reactions, since it has large pore size and surface area. Fig. 2 shows a schematic illustration of the preparation for a manganese oxide with card-house structure from manganese oxide nanosheets. In general, the

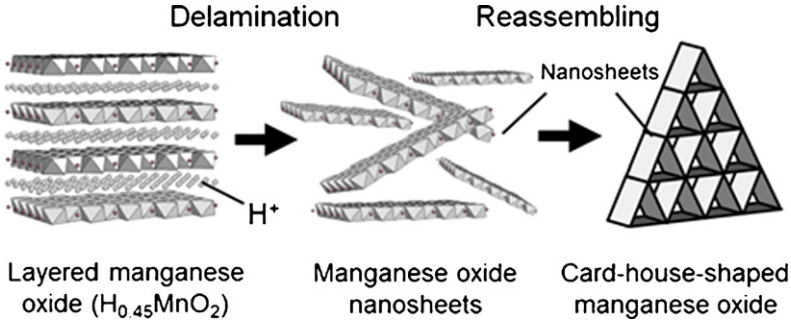

Fig. 2. Schematic illustration of the preparation of a card-house-shaped manganese oxide from manganese oxide nanosheets.

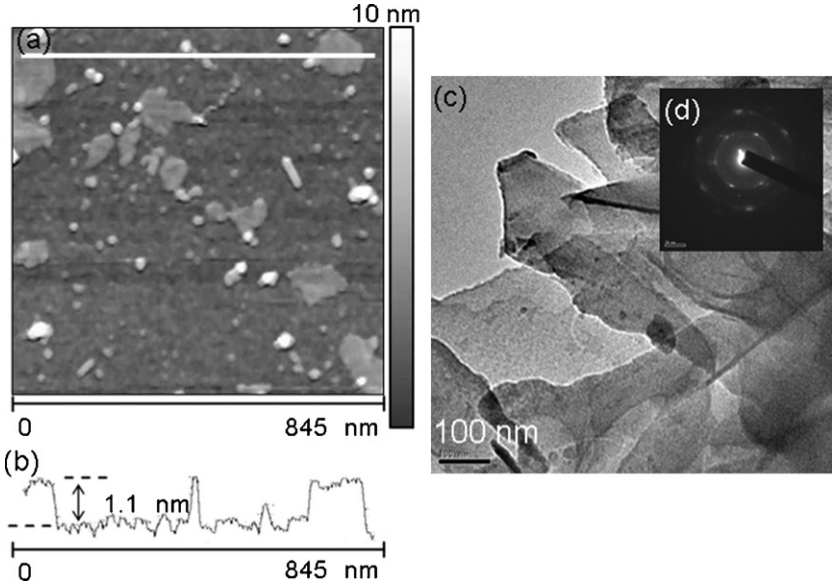

Fig. 3. (a) AFM image; (b) height profile of along the line given in the AFM image; (c) TEM image; and (d) SAED pattern of mono manganese oxide nanosheet.

thickness of a nanosheet is in a molecular size range, while the lateral size ranges from several hundred nanometers to several micrometers [12–14], which makes promising building blocks for the precise fabrication of nano-structures by a bottom-up process [15–17].

Fig. 3a shows an atomic force microscopy (AFM) image of manganese oxide nanosheets. The estimated thickness from the AFM image was approximately 1.1 nm, which is 0.6 nm larger than the theoretical thickness (0.52 nm) of the host layer of the parent layered manganese oxide (Fig. 3b). In general, the thickness of the

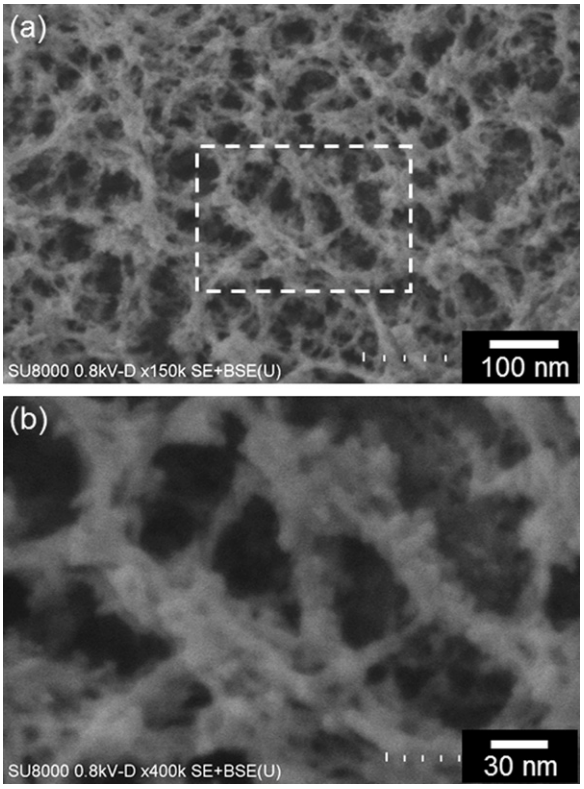

Fig. 4. SEM images of manganese oxide with card-house-like network at; (a) low magnification and (b) high magnification.

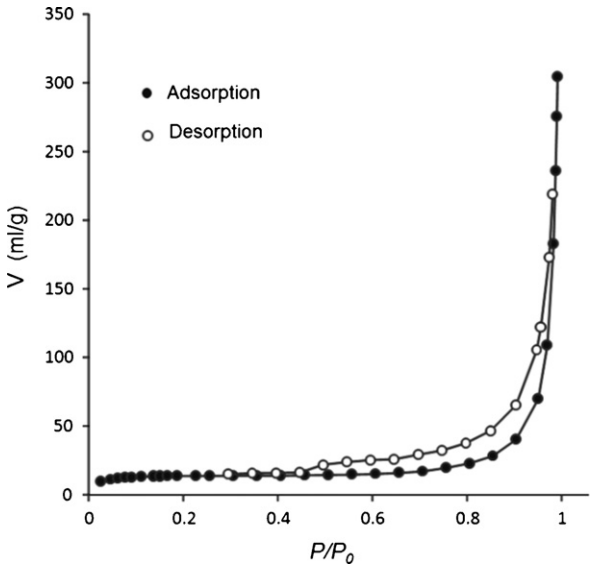

Fig. 5. Nitrogen adsorption–desorption isotherm of manganese oxide.

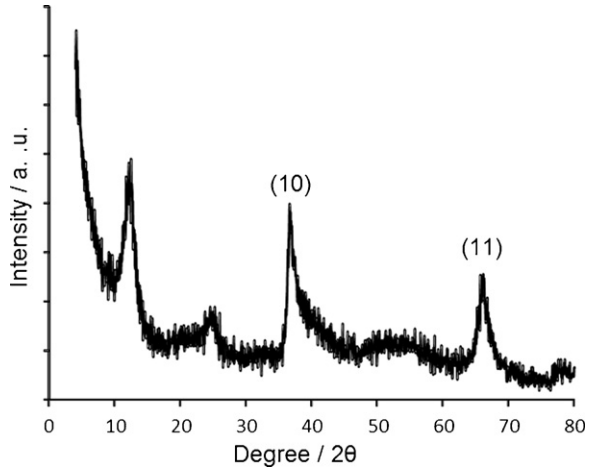

Fig. 6. XRD patterns of manganese oxide with a card-house-like structure.

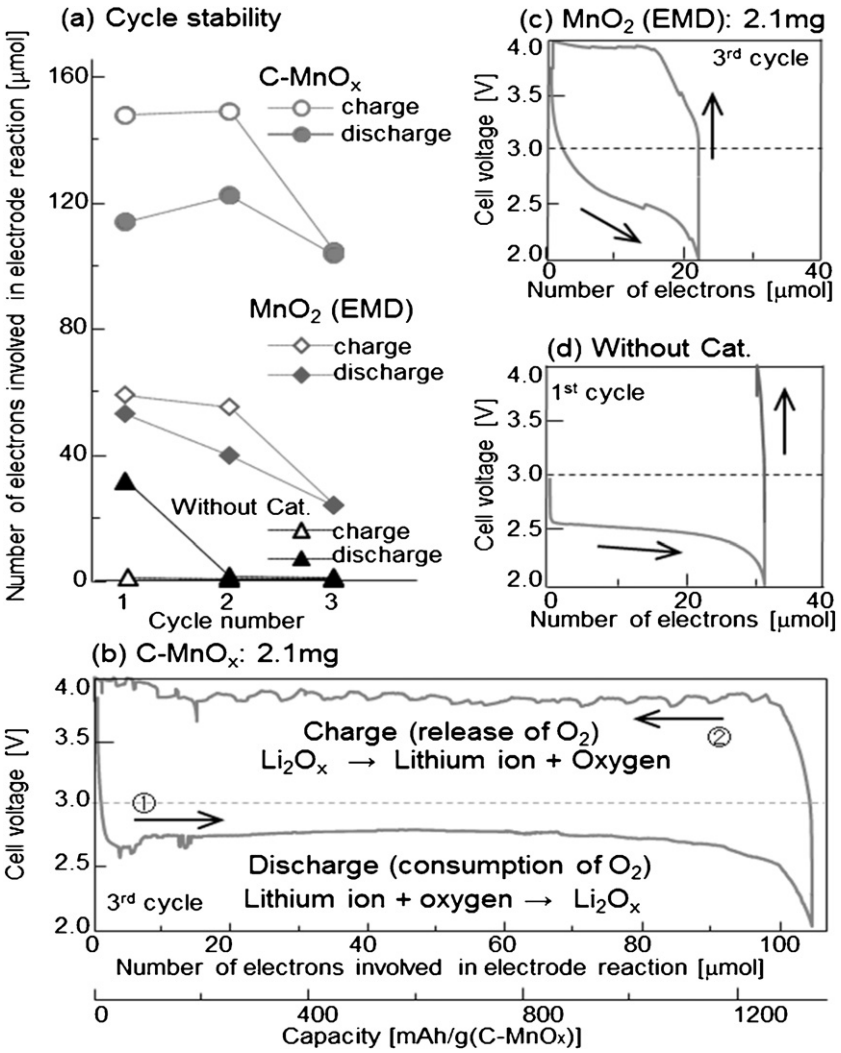

Fig. 7. Cycle stability of charge–discharge reaction (a), and charge–discharge curves for Li-air battery; (b) catalyst: C-MnO_x, (c) catalyst: EMD, and (d) without catalyst (only conducting binder: 5 mg). The cathode electrodes were composed of catalyst (2.1 mg), conducting binder (2.8 mg), and conducting material (0.1 mg). The charge–discharge reactions were performed in pure O_2 atmosphere between 2.0 and 4.0 V at a current density of 0.05 mA cm^{-2}.

oxide nanosheets measured by the AFM is larger than ones estimated from crystallographic data due to absorption of water and amine, and other systematic factors in the AFM measurements. Fig. 3c and d shows a transmission electron microscope (TEM) image and a selected area electron diffraction (SAED) pattern of the manganese oxide nanosheets, respectively. The TEM image shows two-dimensional objects, which can be identified as the manganese oxide nanosheets. The SAED pattern displayed hexagonally arranged spots, indicating that the mono-layer manganese oxide nanosheet is a single crystal and has a two-dimensional hexagonal cell.

Fig. 4 shows the scanning electron microscopy (SEM) images of the manganese oxide powder produced (Fig. 4a). Mesoporous sponge matrix of manganese oxide was observed. There are two pore size ranges existing one with 20–100 nm in width and the other with less 10 nm in width, as shown in Fig. 4b. The porosity of large pores estimated by image analysis of the SEM image was 36%. This manganese oxide with a card-house-like structure is referred to as C-MnO_x.

Fig. 5 shows the nitrogen adsorption–desorption isotherm of the C-MnO_x. The shape of adsorption isotherm was close to II or III type isotherms, and small adsorption hysteresis was observed. The surface area of the C-MnO_x was 49.5 m^2 g^{-1}. Fig. 6 shows the XRD patterns of the C-MnO_x. The peaks at around 12.1° and 24.5° were assigned to basal space between nanosheets. The peaks at around 36.7° and 66.1° were assigned to (1 0) and (1 1) for a hexagonal two-dimensional unit cell with $a = 0.282$ nm. On the other hand, the parent materials, $K_{0.45}MnO_2$, has a rhombohedral system ($R3m$) with cell parameters ($a = 0.2879(2)$ nm, $c = 1.907(1)$ nm) [18]. Thus, the a-axis of the two-dimensional manganese oxide nanosheet slightly shrunk compared to that of the parent layered oxide, although the C-MnO_x maintained the structure of nanosheet. A similar result has been reported for a monolayer film of manganese oxide nanosheets [19].

Fig. 6 shows typical charge–discharge curves (in O_2) and cycle stability of the Li-air battery using the C-MnO_x and electrolytic MnO_2 (EMD) as the catalysts. EMD is known as an effective catalyst for the Li^+/Li_2O_x redox reaction [7]. Fig. 7a shows the cycle stability of the charge–discharge reaction. A large charge–discharge capacity was observed over three cycles with the C-MnO_x system. The numbers of total electrons in the discharge reaction during the initial, second, and third cycles were 148, 149, and 104 μmol, which correspond to 1456, 1562, and 1323 mAh g^{-1} catalyst (C-MnO_x), respectively. These capacities were higher than those for EMD and non-catalyst systems. Fig. 7b and c shows the 3rd charge–discharge cycles using the C-MnO_x and EMD, respectively.

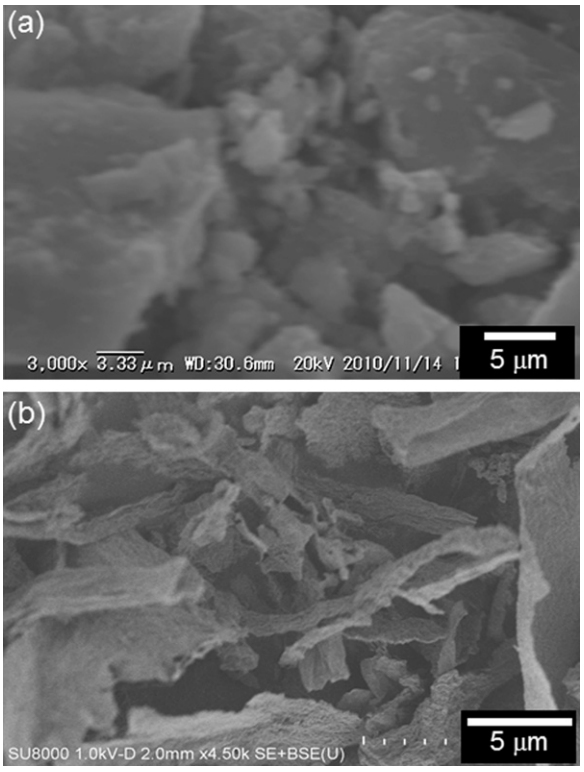

Fig. 8. SEM images of manganese oxides powders obtained by (a) natural dry and (b) freeze dry.

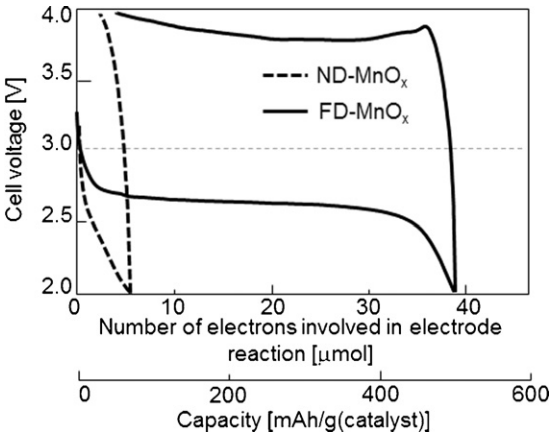

Fig. 9. Charge–discharge curves for Li-air battery using ND-MnO_x (dotted line) and FD-MnO_x (solid line). The cathode electrodes were composed of catalyst (2.1 mg), conducting binder (2.8 mg), and conducting material (0.1 mg). The charge–discharge reactions were performed in pure O_2 atmosphere between 2.0 and 4.0 V at a current density of 0.05 mA cm^{-2}.

The charge–discharge curve for the C-MnO_x displayed a discharge plateau in a large range with the cell voltage, 2.8–2.7 V, while the charge potential plateaued at 3.8 V. The number of electrons involved in the charge–discharge reaction for the electrode with C-MnO_x was 4.7 times larger than that for the electrode containing EMD, where the amounts of the catalyst were same (2.1 mg). This indicates that card-house-like structure with large pore sizes of C-MnO_x might have allowed the greater capacity. When a cathode without manganese oxide was utilized, the numbers of total electrons in the initial discharge reaction was approximately 30 μmol, while the second and third discharge capacities were almost zero as shown in Fig. 7d and a.

The performance of the Li-air battery using manganese oxide with non-card like structure as the cathode catalyst was investigated for comparison. As mentioned previously, two types of manganese oxides with non-card like structure were prepared from the same manganese oxide nanosheets as comparison materials. They were prepared by either naturally drying nanosheet (ND-MnO_x) or by freeze-drying nanosheet (FD-MnO_x). Fig. 8 shows the SEM images of ND-MnO_x and FD-MnO_x. The shape of ND-MnO_x was solid structure (Fig. 8a), while the shape of FD-MnO_x remained in the original sheet structure (Fig. 8b). The BET surface area of ND-MnO_x and FD-MnO_x was 4.9 and 108.1 $m^2\,g^{-1}$. Fig. 9 shows the charge–discharge (first cycle) curves of the Li-air batteries using ND-MnO_x and FD-MnO_x as the cathode catalysts. The discharge capacities for ND-MnO_x and FD-MnO_x were 71 and 502 mAh g^{-1}-catalyst, respectively. Although the FD-MnO_x has larger surface area than the C-MnO_x system (49.5 $m^2\,g^{-1}$), the discharge capacity was lower than the C-MnO_x system. This indicates that the capacities of Li-air batteries are not determined only by the surface area

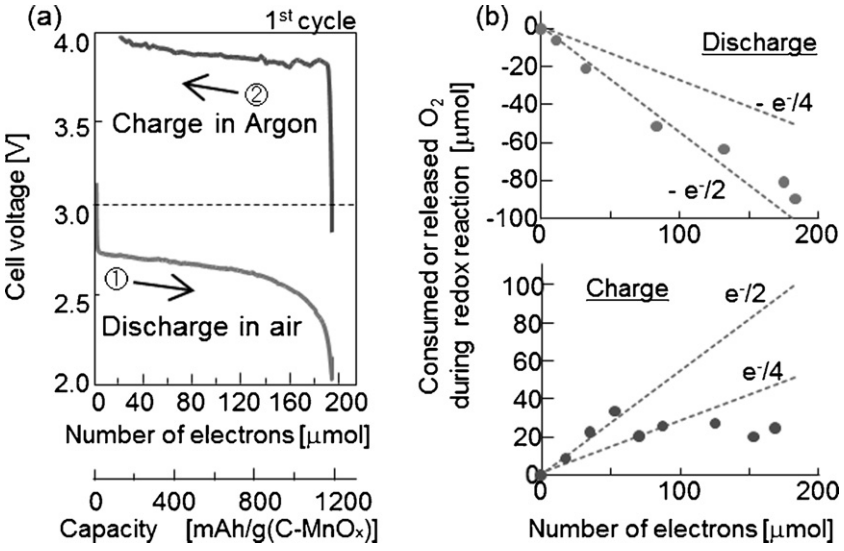

Fig. 10. (a) Discharge (in air) and charge (in argon) curves, (b) the amounts of consumed and released O_2 during the charge–discharge reactions as a function of the number of electron. The cathode electrodes were composed of C-MnO_x (4.2 mg), conducting binder (5.6 mg), and conducting material (0.2 mg). The charge and discharge reactions were performed between 2.0 and 4.0 V at a current density of 0.025 mA cm^{-2} in dry air and Ar atmosphere, respectively.

of the catalyst, but also by the pore sizes of catalysts. The detailed relationship between the pore sizes of the catalyst and the capacity is currently under investigation.

Fig. 10 shows the discharge (in dry air) and charge (in Ar) curves and the amount of O_2 consumed and released during the charge–discharge reaction as a function of the number of electrons. The shapes of the discharge curve in dry air and charge curve in Ar were similar to that in pure O_2 atmosphere, indicating that the C-MnO_x is an effective catalyst in both atmospheres (Fig. 10a). During the discharge reaction, the amount of O_2 gas decreased with the increasing number of electrons involved in the electrode reaction (Fig. 10b). When Li_2O_2 and Li_2O are deposited during the discharge reaction, the ratios of the e^- to O_2 (e^-/O_2) are 2 and 4, respectively. In the C-MnO_x system, the molar ratio (e^-/O_2) was approximately 2, possibly indicating that Li_2O_2 was produced during the discharge reaction. On the other hand, the amount of O_2 released during the charge reaction does not equal to the amount of O_2 consumed during the discharge reaction. Probably, the O_2 generated in the charge reaction cannot easily be released from the matrix of the cathode electrode and electrolyte. The difference in the e^-/O_2 ratios in the charge and discharge reactions is currently under investigation.

4. Conclusion

A manganese oxide with a card-house-like structure was synthesized by reassembling two-dimensional manganese oxide nanosheets, which showed high catalytic activities for Li^+/Li_2O_x ($x = 1, 2$) redox reactions in cathode oxygen electrodes of rechargeable Li-air batteries. The maximum discharge capacity was 1562 mAh g^{-1} catalyst. The molar ratio of the total electrons to the O_2 consumed in the discharge reaction was about 2, indicating Li_2O_2 might be produced in the discharge reaction. Our results indicate that the present manganese oxide is a promising candidate for cathode electrode material in Li-air batteries.

References

[1] K.M. Abraham, Z. Jiang, J. Electrochem. Soc. 143 (1996) 1.
[2] P.G. Bruce, Solid State Ionics 179 (2008) 752.
[3] M. Armand, J.M. Tarascon, Nature 451 (2008) 652.
[4] G. Girishkumar, B. McCloskey, A.C. Luntz, S. Swanson, W. Wilcke, J. Phys. Chem. Lett. 1 (2010) 2193.
[5] J. Read, J. Electrochem. Soc. 149 (2002) A1190.
[6] J. Read, K. Mutolo, M. Ervin, W. Behl, J. Wolfenstine, A. Driedger, D. Foster, J. Electrochem. Soc. 150 (2003) A1351.
[7] T. Ogasawara, A. Débart, M. Holfazel, P. Novák, P.G. Bruce, J. Am. Chem. Soc. 128 (2006) 1390.
[8] A. Débart, A.J. Paterson, J. Bao, P.G. Bruce, Angew. Chem. Int. Ed. 47 (2008) 4521.
[9] A.K. Thapa, K. Saimen, T. Ishihara, Electrochem. Solid State Lett. 13 (2010) A165.
[10] A.K. Thapa, T. Ishihara, J. Power Sources 196 (2011) 7016.
[11] Y.-C. Lu, Z. Xu, H.A. Gasteiger, S. Chen, K. Hamad-Schifferli, Y. Shao-Horn, J. Am. Chem. Soc. 132 (2010) 12170.
[12] Y. Omomo, T. Sasaki, L. Wang, M. Watanabe, J. Am. Chem. Soc. 125 (2003) 3568.
[13] R.E. Schaak, T.E. Mallouk, Chem. Mater. 12 (2000) 2513.
[14] S. Ida, C. Ogata, U. Unal, K. Izawa, T. Inoue, O. Altuntasoglu, Y. Matsumoto, J. Am. Chem. Soc. 129 (2007) 8956.
[15] M. Fang, C.H. Kim, G.B. Saupe, H.-N. Kim, C.C. Waraksa, T. Miwa, A. Fujishima, T.E. Mallouk, Chem. Mater. 11 (1999) 1526.
[16] L. Li, R. Ma, Y. Ebina, K. Fukuda, K. Takada, T. Sasaki, J. Am. Chem. Soc. 129 (2007) 8000.
[17] S. Ida, Y. Sonada, K. Ikeue, Y. Matsumoto, Chem. Commun. 46 (2010) 877.
[18] P.C. Delmas, C. Fouassier, Z. Anorg. Allg. Chem. 420 (1976) 184.
[19] K. Fukuda, I. Nakai, Y. Ebina, M. Tanaka, T. Mori, T. Sasaki, J. Phys. Chem. B 110 (2006) 17070.